(Received 11 June 2024, Accepted 15 July 2024, Scheduled 21 July 2024)

Mode Control of Slotline Resonator and Its Application to the Design of Balanced BPF with Ultra-Wide Stopband

Jia-Qi Wang[1, 2] and Feng Wei[1, 2, *]

[1] *The National Key Laboratory of Radar Detection and Sensing, Xian 710071, China*
[2] *School of Electrical Engineering, Xidian University, Xi'an 710071, China*

ABSTRACT: In this paper, a mode control technology of a slotline resonator is proposed and utilized to guide the design of the slotline resonator. With this method, characteristic modes generated by the slotline resonator are more controllable. With characteristic mode analysis, which is the core of this technology, the desired and unwanted modes of the slotline resonator are easy to be analyzed, controlled, and further used to expand the stopband bandwidth. By applying this technology, a multi-mode slotline resonator with a T-shaped coupling structure (MMSR-T) is proposed by modifying a multi-mode slotline resonator (MMSR), and its unwanted modes out of the passband are more controllable without influencing the expected modes in the passband. Based on the proposed MMSR-T, a balanced bandpass filter (BPF) is proposed, which consists of a U-shaped microstrip/slotline transition as the input/output structure, a T-shaped slotline feeding structure as a feeding terminal, and MMSR-T as the filtering unit. Through the mode analysis and design of MMSR-T, ultra-wide differential-mode (DM) stopband, high common-mode (CM) suppression, and high DM selectivity are obtained in this design. The measured results agree well with the theoretical predictions and simulated results. The effects of mode control technology on stopband extension are proven.

1. INTRODUCTION

In traditional radio-frequency (RF) receiver front-end circuit, bandpass filter (BPF) with low insertion loss (IL) is needed between the antenna and low noise amplifier (LNA). However, since passband characteristics of the distributed filter are periodic, parasitic passbands are generated at higher frequencies, thereby the stopband bandwidth is limited [1–3]. Consequently, the high-frequency and high-power signals can accidentally enter the receiving system to destroy LNA and post-stage RF circuits. Therefore, the filter with a high rejection level and wide stopband is needed.

In the past few years, lots of methods have been introduced to design BPF with wide stopband. The single-band [4–8] and dual-band [9] microstrip filters with wide stopband were proposed with good in-band performance and low insertion loss. However, affected by the high-order harmonics, the stopband bandwidth and rejection level of these designs are limited. In [10], a step impedance resonator (SIR) was first proposed, and its resonance modes can be controlled by adjusting the impedance ratio and electrical length ratio. After that, single-band [11, 12] and dual-band [13–15] BPFs with wide stopband were designed. However, their applications are limited by the poor selectivity. Therefore, a better wide-stopband design process needs to be further investigated.

On the other hand, compared with single-ended RF front-end circuits, balanced ones [16] are important in the wireless communication system because of their high immunity to environmental noise. In the past few years, some balanced passive and active components, such as balanced filters [17], balanced antennas [18], and balanced amplifiers [19] have been proposed. In [20] and [21], balanced wide DM passband BPFs based on branch-line structures with additionally attached stubs were designed. In [22], CM signal transmission can be suppressed without affecting DM performance by utilizing a series-LC resonant structure below the folded SIR. Meanwhile, to enhance the CM suppression, the transversal signal-interference theory was proposed in [23, 24]. However, poor selectivity and narrow DM stopband limit their further application. To prevent the interferences, balanced BPFs with high selectivity and ultra-wide stopband need to be further researched.

In this paper, a mode control technology of the slotline resonator is proposed to realize ultra-wide stopband in balanced design. The specific design process is as follows:

1) Appropriately design a resonator based on the expected frequency. Use characteristic mode analysis to simulate the characteristic modes.

2) Choose the desired and unwanted modes.

3) Analyze the E-field distribution under different modes and optimize the structure of the slotline resonator to change the characteristics modes generated by the slotline resonator.

4) Design the feeding structure to suppress the unwanted modes without influencing the excitation of the desired modes.

The proposed mode control technology reveals the underlying mechanisms of control of all modes and research unprecedented stopband extension. Through the detailed E-field distribution analysis and the proposed mode control technology, the effects of the structure of the multi-mode slotline resonator (MMSR) on characteristic modes are analyzed and utilized to

* Corresponding author: Feng Wei (fwei@mail.xidian.edu.cn).

extend the stopband. Therefore, the underlying mechanism of mode control is comprehensively revealed, and the mode excitation and suppression are clearly guided. In this paper, the proposed technology guides the transformation of MMSR to a multi-mode slotline resonator with a T-shaped coupling structure (MMSR-T), significantly distinguishing the desired and unwanted modes. With further specific analysis of the E-field distribution, the design requirements of the feeding structure are clarified and achieved, suppressing the unwanted modes without influencing the desired modes of excitation. Consequently, the stopband bandwidth is greatly extended, and a balanced BPF is designed. The proposed design consists of a microstrip/slotline transition structure, a T-shaped slotline feeding structure, and MMSR-T. The rectangle coefficient of 3 dB to 25 dB is 0.85. A stopband bandwidth with a rejection level of 15 dB reaches up to 5.57 times the center frequency. Meanwhile, the CM suppression level is better than 47 dB for the DM passband.

2. MODE CONTROL TECHNOLOGY

2.1. Mode Analysis

With the characteristic mode analysis, characteristic modes of arbitrary-shaped resonators can be obtained directly. Meanwhile, the desired and unwanted modes can be clarified.

Figure 1 shows a multi-mode slotline resonator (MMSR), which integrates a half-wave-length slotline resonator, an open slotline stub, and a spiral-short-ended slotline stub, which are denoted as A, B, and C, respectively. The lengths of half A, B, and C are L_A, L_B, and L_C, respectively. With the characteristic mode analysis, six modes generated by MMSR and the corresponding E-field distributions from DC to 15 GHz are obtained and shown in Table 1. The arrows suggest the direction of the E-field of each mode.

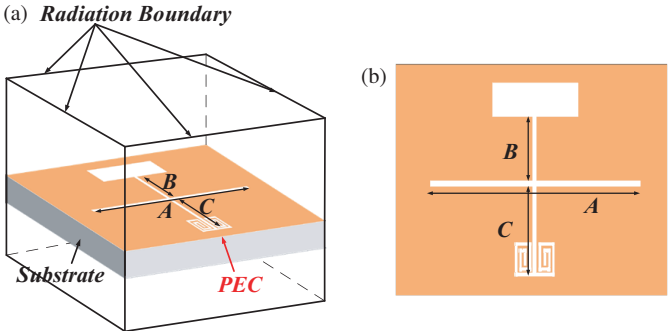

FIGURE 1. Geometrical model of MMSR. (a) Boundary setup. (b) Top view.

For mode 1, the E-field energy is primarily concentrated on A and B, and its directions on both arms of A are reversed. The electric lengths of B and half A can be considered as quarter-wavelength at f_1. Therefore, when the admittance of A is equal to twice that of B, the formula for mode 1's characteristic frequency can be expressed as

$$f_1 = \frac{c}{4\left(L_A + L_B\right)\sqrt{\varepsilon_{eff}}} \tag{1}$$

TABLE 1. E-field distributions of characteristic modes generated by MMSR.

	Mode 1 (2.93 GHz)	Mode 2 (3.82 GHz)
E-fields (V/m) Max Min	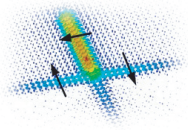	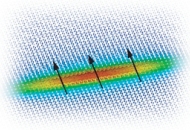
	Mode 3 (4.35 GHz)	Mode 4 (9.2 GHz)
E-fields (V/m) Max Min	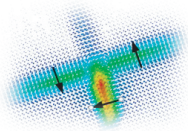	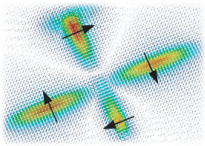
	Mode 5 (12.3 GHz)	Mode 6 (12.5 GHz)
E-fields (V/m) Max Min	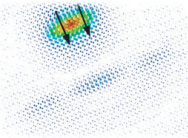	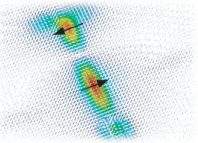

where c denotes the speed of light in free space, and ε_{eff} is the effective permittivity. It can be observed that mode 1 is not affected by the loaded spiral-short-ended slotline stub.

Similar to the analysis process of mode 1, modes 2 and 3 can be adjusted independently by L_A and L_C, respectively. Moreover, the characteristic frequencies of modes 2 and 3 can be summarized as

$$f_2 = \frac{c}{4L_A\sqrt{\varepsilon_{eff}}} \tag{2}$$

$$f_3 = \frac{c}{4(L_A + L_C)\sqrt{\varepsilon_{eff}}} \tag{3}$$

Based on the above analysis, modes 1, 2, and 3 can be controlled flexibly and independently, thereby these three modes are excited to generate the DM passband. Based on the E-field distributions of the stubs, these three modes can be excited simultaneously only when stub A is fed.

The rest of modes 4, 5, and 6 are undesirable modes as their resonance frequencies deviate from the expected passband, producing high-order harmonics. For mode 4, the E-field energy is mainly distributed on A, B, and C. For mode 5, the E-field energy is mainly distributed on the open end. For mode 6, the E-field is mainly distributed on B and C. Therefore, it is needed to ensure that the unwanted modes 4, 5, and 6 are not excited when stub A is fed. Next, by improving the structure of the MMSR, all unwanted modes will not resonate on stub A, thereby suppressing unnecessary modes and forming a wider stopband.

2.2. Mode Control and Suppression of Unwanted Modes

To realize the control of all modes, MMSR is modified and MMSR-T is proposed, which is realized by adding a pair of stubs D perpendicular to both sides of stub A in the structure of MMSR, as shown in Fig. 2. The proposed MMSR-T integrates a half-wavelength slotline resonator, an open slotline stub, a spiral-short-ended slotline stub, and the T-shaped slotline coupling structure which are denoted as A, B, C, and D, respectively. The lengths of half A, B, C, and half D are L_A, L_B, L_C, and L_D, respectively. As shown in Table 2, different from MMSR, there are five unwanted modes generated by MMSR-T from DC to 15 GHz.

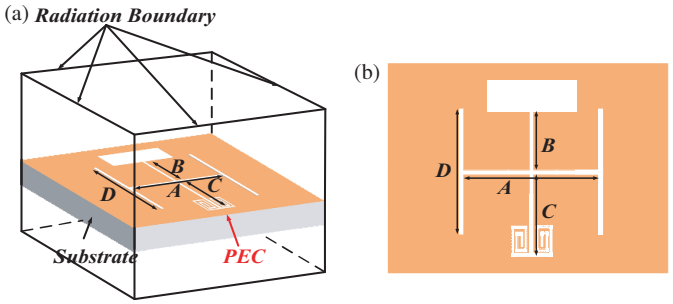

FIGURE 2. Geometrical model of MMSR-T. (a) Boundary setup. (b) Top view.

In these modes, the E-field distributions for modes 1, 2, and 3 are similar between MMSR-T and MMSR to design the passband. The frequencies of the corresponding characteristic mode are as follows:

$$f_1 = \frac{c}{4\left(L_D + L_A + L_B\right)\sqrt{\varepsilon_{eff}}} \tag{4}$$

$$f_2 = \frac{c}{4(L_A + L_D)\sqrt{\varepsilon_{eff}}} \tag{5}$$

$$f_3 = \frac{c}{4(L_D + L_A + L_C)\sqrt{\varepsilon_{eff}}} \tag{6}$$

The remaining modes are unwanted modes because they are outside the passband. For mode 4, the E-field energy is mainly distributed on B and C. The E-field energy of mode 8 is similar to mode 4. For mode 7, the E-field energy is mainly distributed on the open end. For mode 5, the E-field energy is mainly distributed on D. And the E-fields on both ends of D are in the same direction. Mode 6 is similar to mode 5.

All characteristic modes in the passband produce E-field distribution with unique characteristics compared with other undesired modes. For mode 1, the E-field distributions on two ends of the D are opposite. Similar to mode 1, the E-field distributions of modes 2 and 3 exhibit the same characteristics. Since stubs A and D form the T-shaped slotline coupling structure, only modes 1, 2, and 3 generate an opposite E-field on both ends of D. With the T-shaped slotline feeding structure shown in Fig. 3(a), the E-field required for modes 1, 2, and 3 is provided, and the flexibly controllable passband can be designed.

In the stopband design, Figs. 3(b), (c), and (d) show the E-filed distribution of the rest of the modes on the feeding terminal. As shown in Fig. 3(b), there is little or none of energy

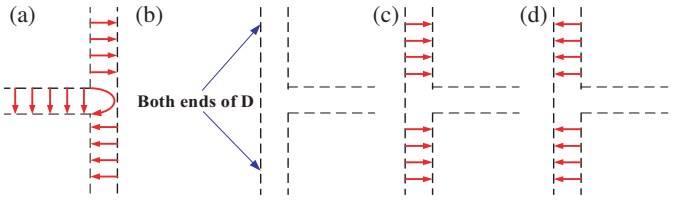

FIGURE 3. (a) Layout and E-field distribution of the T-shaped slotline feeding structure. E-field distribution on both ends of D for (b) modes 4, 7, 8, (c) 5, and (d) 6.

distributed on both ends of D for modes 4, 7, and 8. Therefore, these three modes cannot be excited by the T-shaped slotline feeding structure. As shown in Fig. 3(c), the E-field required for mode 5 to be excited has the same direction on both ends of D. However, the T-shaped slotline feeding structure can only provide the E-field shown in Fig. 3(a). The distribution of the E-fields shown in Figs. 3(c) and (d) cannot be provided by the T-shaped slotline feeding structure. These two modes are also inhibited.

Figure 4 depicts the illustration of the high-order mode suppression. Only modes 1, 2, and 3 are excited to generate the expected passband. Modes 4, 5, 6, 7, and 8 are inhibited. At the same time, a wide stopband is achieved. The effectiveness of the modification from MMSR to MMSR-T is validated. Compared to the traditional design methods, with this mode control technology, the design requirements of the feeding structure are significantly clarified to further achieve better stopband performance.

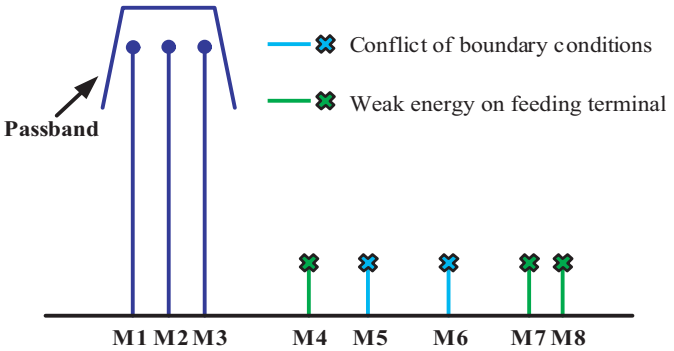

FIGURE 4. Illustration of the high-order modes suppression. (M* denotes mode *.

2.3. Balanced BPF with Ultra-Wide Stopband

In order to simplify the wide stopband design process, mode control technology based on the characteristic mode analysis is innovatively adopted to design a balanced BPF with ultra-wide DM stopband. As given in Fig. 5(a), the designed balanced BPF consists of balanced input/output U-shaped microstrip lines, MMSR-T, and a T-shaped slotline feeding structure. By introducing U-shaped balanced input/output ports, all CM signals are prevented into the resonator, and only the DM responses need to be considered. Four shielded strips are employed to enhance the coupling between the T-shaped slotline couple structures.

TABLE 2. E-field distributions of characteristic modes generated by MMSR-T.

	Mode 1 (2.9 GHz)	Mode 2 (3.8 GHz)	Mode 3 (4.3 GHz)	Mode 4 (8.9 GHz)
	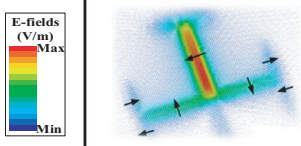			
	Mode 5 (9.2 GHz)	Mode 6 (9.9 GHz)	Mode 7 (11.6 GHz)	Mode 8 (12 GHz)
	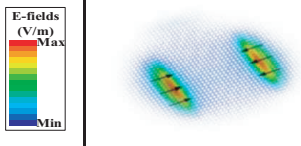			

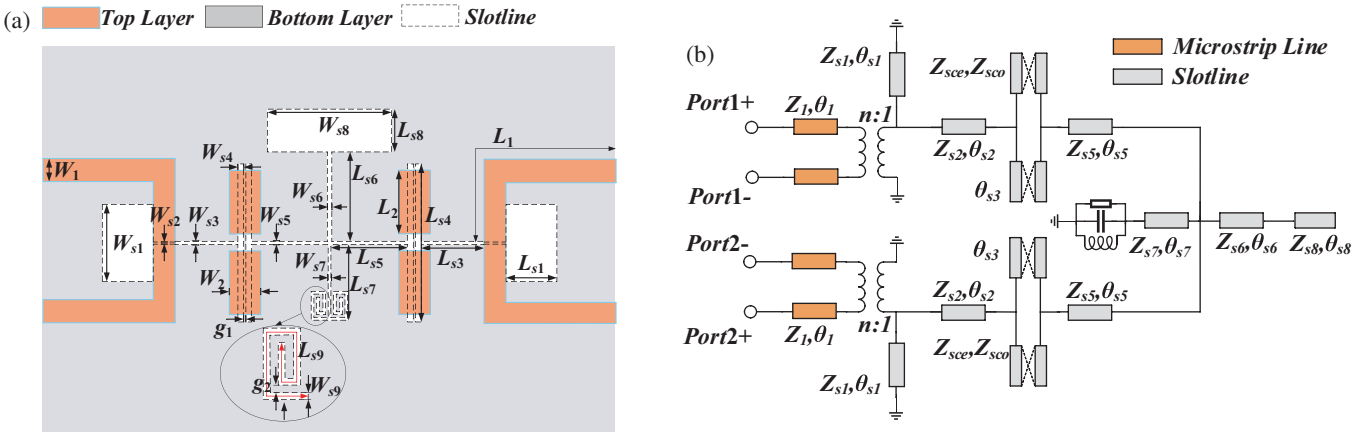

FIGURE 5. (a) Layout of the designed balanced BPF. ($W_1 = 2.4$, $W_2 = 1.8$, $W_{s1} = 7.5$, $W_{s2} = 0.1$, $W_{s3} = 0.2$, $W_{s4} = 0.2$, $W_{s5} = 0.1$, $W_{s6} = 0.2$, $W_{s7} = 0.1$, $W_{s8} = 9.8$, $W_{s9} = 0.1$, $L_1 = 16.5$, $L_2 = 4.6$, $L_{s1} = 2.9$, $L_{s3} = 6.9$, $L_{s4} = 11.8$, $L_{s5} = 4.2$, $L_{s6} = 9.5$, $L_{s7} = 7.5$, $L_{s8} = 1.9$, $L_{s9} = 3.2$, $g_1 = 0.1$, and $g_2 = 0.1$, all in millimeters.) (b) DM equivalent circuit of the proposed balanced BPF.

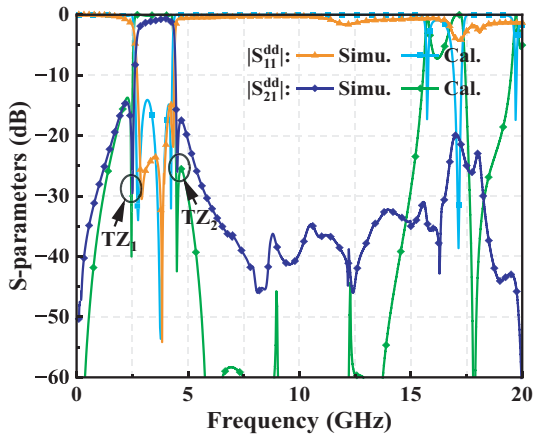

FIGURE 6. Calculated and simulated DM responses of the proposed BPF with ultra-wide DM stopband.

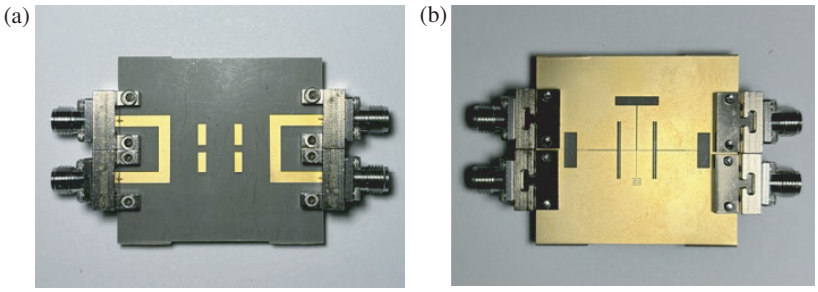

FIGURE 7. Photographs of the fabricated balanced BPF. (a) Top view. (b) Bottom view.

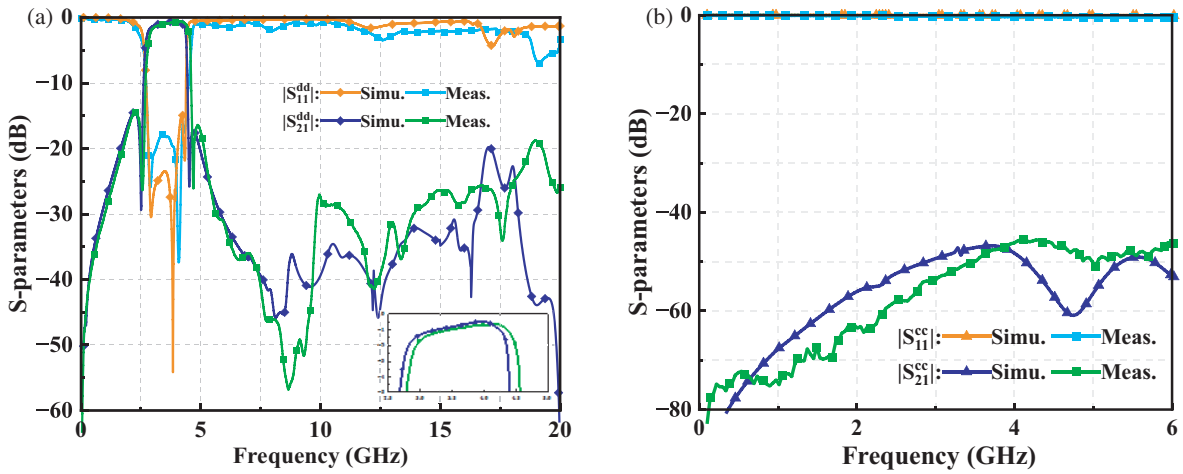

FIGURE 8. EM-simulated and measured results of the proposed BPF with ultra-wide DM stopband. (a) DM transmission results. (b) CM transmission results.

TABLE 3. Comparison with other prior-art works.

Ref.	IL (dB)	CM suppression (dB)	DM Stopband (dB)	Size (λ_g^2)	$\Delta f_{3\,\mathrm{dB}}/\Delta f_{25\,\mathrm{dB}}$
[4]	1	> 28	22 dB@ $> 3.6f_0$	0.245	0.65
[5]	4	> 30	20 dB@ $> 2f_0$	0.292	0.66
[6]	1.01	No	20 dB@ $> 3.9f_0$	0.005	0.33
[7]	1.33	No	20 dB@ $> 1.11f_0$	3.31	0.31
[8]	2.91	No	25 dB@ $> 2.1f_0$	1.86	0.45
[16]	0.8	No	15 dB@ $> 1.42f_0$	0.108	0.92
[17]	0.5	> 33.7	21.2 dB@ $> 3.04f_0$	0.31	0.71
This Design	**0.6**	**> 47**	**15 dB@ $> 5.57f_0$**	**0.162**	**0.85**

Figure 5(b) shows the DM equivalent circuit of the proposed balanced filter. Due to the replacement between the transmission line model and slotline model in ADS, there are some differences between the calculated results and simulated ones. In this paper, the transition between the microstrip line and slotline is expressed as an equivalent transformer.

Figure 6 shows the comparison between the calculated results and simulated ones, which are obtained by ADS and HFSS, respectively. The first TZ (TZ_1), which is generated by the open slotline stub, contributes to improving the selectivity of the lower passband. The second TZ (TZ_2), which is determined by the spiral-short-ended slotline stub, controls the higher cut-off frequency. TZ_1 and TZ_2 can be independently controlled by L_{s8} and L_{s9}, respectively.

2.4. Simulation and Measurement

According to the above analysis, a balanced BPF with a center frequency at 3.48 GHz is designed and fabricated. Based on the above analysis, f_1, f_2, and f_3 are selected at 2.90 GHz, 3.84 GHz, and 4.32 GHz, respectively. The overall size of the filter is 33.9×18.8 mm ($0.54\lambda_g \times 0.30\lambda_g$, λ_g is the guided wavelength at the center frequency). Photographs of the fabricated balanced BPF are shown in Fig. 7.

Figure 8 exhibits the measured and simulated S-parameters of the designed BPF. The measured DM center frequency is 3.59 GHz, and the measured minimum DM IL is 0.6 dB. At the same time, the 3-dB DM fractional bandwidth is 44.52%, and the DM return loss is greater than 15 dB. Two TZs are located at 2.48 GHz and 4.50 GHz, respectively. The rectangle coefficient of 3 dB to 25 dB is 0.85, which indicates that DM high selectivity is obtained in this design. Furthermore, the DM stopband reaches up to 5.57 times of the center frequency with a rejection level of 15 dB, and the 25 dB DM stopband rejection level is achieved from 6 GHz to 16 GHz. Meanwhile, the CM suppression level is better than 47 dB for the DM passband.

According to Table 3, a wider DM stopband is realized in this design. Meanwhile, high CM suppression and good selectivity are achieved. The design process is based on the characteristic mode analysis, which makes this design more attractive.

3. CONCLUSION

In this work, the application of characteristic mode analysis is significantly expanded beyond its traditional uses. A new mode control technology specifically designed for the slotline resonators is presented. As a core of this technology, characteristic mode analysis is used to analyze the characteristic modes of the proposed slotline resonators, further clarifying the desired modes suitable for flexible passband design and unwanted modes that require suppression. Through the E-field analysis of all modes, the modification of the slotline resonator is

guided, and the design requirement of the feeding structure is further clarified. Consequently, the original unwanted modes are suppressed without influencing the excitation of desired modes. Thereby, the stopband is significantly extended. To verify the correctness of this technology, a balanced BPF with steep DM selectivity, ultra-wide DM stopband, and high CM suppression is designed and fabricated. The simulation and measurement show a good agreement.

REFERENCES

[1] Chen, J.-X., J. Li, Y. Zhan, W. Qin, J. Shi, and Z.-H. Bao, "Design of balanced and balun filters using dual-mode cross-shaped dielectric resonators," *IEEE Transactions on Microwave Theory and Techniques*, Vol. 65, No. 4, 1226–1234, Apr. 2017.

[2] Zhu, H., X. Zhu, Y. Yang, and Y. Sun, "Design of miniaturized on-chip bandpass filters using inverting-coupled inductors in (Bi)-CMOS technology," *IEEE Transactions on Circuits and Systems I: Regular Papers*, Vol. 67, No. 2, 647–657, Feb. 2020.

[3] Gómez-García, R., J.-M. Muñoz-Ferreras, and D. Psychogiou, "Adaptive multi-band negative-group-delay RF circuits with low reflection," *IEEE Transactions on Circuits and Systems I: Regular Papers*, Vol. 68, No. 5, 2196–2209, May 2021.

[4] Sans, M., J. Selga, P. Vélez, J. Bonache, A. Rodríguez, V. E. Boria, and F. Martín, "Compact wideband balanced bandpass filters with very broad common-mode and differential-mode stopbands," *IEEE Transactions on Microwave Theory and Techniques*, Vol. 66, No. 2, 737–750, Feb. 2018.

[5] Liu, X., Z. Zhu, Y. Liu, Q. Lu, X. Yin, and Y. Yang, "Compact bandpass filter and diplexer with wide-stopband suppression based on balanced substrate-integrated waveguide," *IEEE Transactions on Microwave Theory and Techniques*, Vol. 69, No. 1, 54–64, Jan. 2021.

[6] Xu, W., K. Ma, and Y. Guo, "Design of miniaturized 5G SISL BPFs with wide stopband using differential drive inductor resonators," *IEEE Transactions on Microwave Theory and Techniques*, Vol. 70, No. 6, 3115–3124, Jun. 2022.

[7] Zhang, G., X. Zhou, K.-D. Xu, J. Yang, X. Sun, B. Xu, K.-W. Tam, S. Feng, W. Tang, and J. Hong, "Design of wide-stopband and dual-band filtering crossovers based on mixed substrate integrated waveguide cavities," *IEEE Transactions on Microwave Theory and Techniques*, Vol. 71, No. 12, 5346–5357, Dec. 2023.

[8] Zhou, K., C.-X. Zhou, and W. Wu, "Resonance characteristics of substrate-integrated rectangular cavity and their applications to dual-band and wide-stopband bandpass filters design," *IEEE Transactions on Microwave Theory and Techniques*, Vol. 65, No. 5, 1511–1524, May 2017.

[9] Tang, D., C. Han, Z. Deng, H. J. Qian, and X. Luo, "Substrate-integrated defected ground structure for single-and dual-band bandpass filters with wide stopband and low radiation loss," *IEEE Transactions on Microwave Theory and Techniques*, Vol. 69, No. 1, 659–670, Jan. 2021.

[10] Sagawa, M., K. Takahashi, and M. Makimoto, "Miniaturized hairpin resonator filters and their application to receiver front-end MICs," *IEEE Transactions on Microwave Theory and Techniques*, Vol. 37, No. 12, 1991–1997, Dec. 1989.

[11] Sheikhi, A., A. Alipour, and A. Mir, "Design and fabrication of an ultra-wide stopband compact bandpass filter," *IEEE Transactions on Circuits and Systems II: Express Briefs*, Vol. 67, No. 2, 265–269, Feb. 2020.

[12] Kumar, L. and M. S. Parihar, "A wide stopband low-pass filter with high roll-off using stepped impedance resonators," *IEEE Microwave and Wireless Components Letters*, Vol. 28, No. 5, 404–406, May 2018.

[13] Tang, J., H. Liu, and Y. Yang, "Compact wide-stopband dual-band balanced filter using an electromagnetically coupled SIR pair with controllable transmission zeros and bandwidths," *IEEE Transactions on Circuits and Systems II: Express Briefs*, Vol. 67, No. 11, 2357–2361, Nov. 2020.

[14] Zhao, X.-B., F. Wei, P. F. Zhang, and X. W. Shi, "Mixed-mode magic-Ts and their applications on the designs of dual-band balanced out-of-phase filtering power dividers," *IEEE Transactions on Microwave Theory and Techniques*, Vol. 71, No. 9, 3896–3905, Sep. 2023.

[15] Shi, J. and Q. Xue, "Dual-band and wide-stopband single-band balanced bandpass filters with high selectivity and common-mode suppression," *IEEE Transactions on Microwave Theory and Techniques*, Vol. 58, No. 8, 2204–2212, Aug. 2010.

[16] Zhu, H., A. M. Abbosh, and L. Guo, "Wideband four-way filtering power divider with sharp selectivity and wide stopband using looped coupled-line structures," *IEEE Microwave and Wireless Components Letters*, Vol. 26, No. 6, 413–415, Jun. 2016.

[17] Li, Z., F. Wei, B. Liu, and X. W. Shi, "Design of balanced wideband bpf based on tri-mode slotline resonators," *IEEE Transactions on Circuits and Systems II: Express Briefs*, Vol. 69, No. 6, 2767–2771, Jun. 2022.

[18] Shen, C., W.-J. Lu, and L. Zhu, "Planar self-balanced magnetic dipole antenna with wide beamwidth characteristic," *IEEE Transactions on Antennas and Propagation*, Vol. 67, No. 7, 4860–4865, Jul. 2019.

[19] Cao, Y., H. Lyu, and K. Chen, "Continuous-mode hybrid asymmetrical load-modulated balanced amplifier with three-way modulation and multi-band reconfigurability," *IEEE Transactions on Circuits and Systems I: Regular Papers*, Vol. 69, No. 3, 1077–1090, Mar. 2022.

[20] Lim, T. B. and L. Zhu, "A differential-mode wideband bandpass filter on microstrip line for UWB application," *IEEE Microwave and Wireless Components Letters*, Vol. 19, No. 10, 632–634, Oct. 2009.

[21] Lim, T. B. and L. Zhu, "Differential-mode ultra-wideband bandpass filter on microstrip line," *Electronics Letters*, Vol. 45, No. 22, 1124–1125, Oct. 2009.

[22] Fernández-Prieto, A., J. Martel, F. Medina, F. Mesa, and R. R. Boix, "Compact balanced fsir bandpass filter modified for enhancing common-mode suppression," *IEEE Microwave and Wireless Components Letters*, Vol. 25, No. 3, 154–156, Mar. 2015.

[23] Shi, S., W.-W. Choi, W. Che, K.-W. Tam, and Q. Xue, "Ultra-wideband differential bandpass filter with narrow notched band and improved common-mode suppression by DGS," *IEEE Microwave and Wireless Components Letters*, Vol. 22, No. 4, 185–187, Apr. 2012.

[24] Wu, X.-H. and Q.-X. Chu, "Compact differential ultra-wideband bandpass filter with common-mode suppression," *IEEE Microwave and Wireless Components Letters*, Vol. 22, No. 9, 456–458, Sep. 2012.